Citation for final published version:

Yu, Yanke, Miao, Jifa, He, Chi, Chen, Jinsheng, Li, Can and Douthwaite, Mark 2018. The remarkable promotional effect of SO_2 on Pb-poisoned V_2O_5-WO_3/TiO_2 catalysts: An in-depth experimental and theoretical study. Chemical Engineering Journal 338 , pp. 191-201. 10.1016/j.cej.2018.01.031

Publishers page: http://dx.doi.org/10.1016/j.cej.2018.01.031

The remarkable promotional effect of SO_2 on Pb-poisoned V_2O_5-WO_3/TiO_2 catalysts: An in-depth experimental and theoretical study

Yanke Yu[a], Jifa Miao[b], Chi He[a,c], , Jinsheng Chen[b], , Can Li[d], Mark Douthwaite[c]

[a] Department of Environmental Science and Engineering, State Key Laboratory of Multiphase Flow in Power Engineering, School of Energy and Power Engineering, Xi'an Jiaotong University, Xi'an 710049, PR China
[b] Center for Excellence in Regional Atmospheric Environment, Institute of Urban Environment, Chinese Academy of Sciences, Xiamen 361021, China
[c] Cardiff Catalysis Institute, School of Chemistry, Cardiff University, Main Building, Park Place, Cardiff CF10 3AT, UK
[d] Center for Coordination Bond Engineering, College of Materials Science and Engineering, China Jiliang University, Hangzhou 310018, China

HIGHLIGHTS

- SO_2 increased the activity of Pb-poisoned commercial V-based SCR catalysts.
- SO_2 recovered the Brønsted acid sites on surface of the Pb-poisoned catalyst.
- A surface bidentate sulfate was formed on surface of the Pb-poisoned catalyst.
- Adsorption of SO_2 and NH_3 on surface was studied by DFT.

GRAPHICAL ABSTRACT

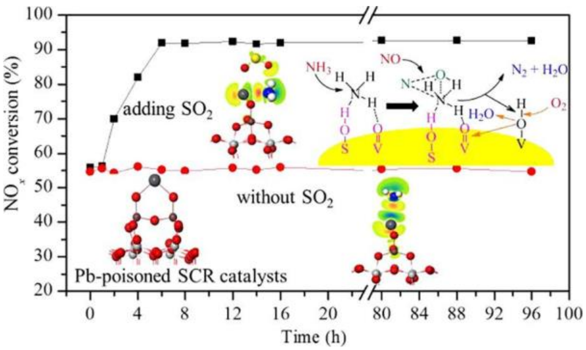

ARTICLE INFO

Keywords:
SCR catalysts
Pb
Brønsted acid sites
Bidentate sulfate
DFT

ABSTRACT

Currently, Pb poisoning of heterogeneous catalysts is considered to be a key area of interest in research involved with industrial NO_x reduction. As such, a series of Pb-poisoned V_2O_5-WO_3/TiO_2 catalysts were prepared by a wet impregnation method and the influence of SO_2 on the performance of these poisoned catalysts for NO_x reduction was assessed both experimentally and using theoretical calculations. As expected, the incorporation of Pb in these materials resulted in a significant reduction in their catalytic performance. The conversion of NO_x over the Pb-V_2O_5-WO_3/TiO_2 catalyst increased from approximately 50% to 90% in presence of SO_2 (2000 ppm) at 350 °C. It was postulated that in the absence of SO_2, Pb reacts with surface V-OH species, which ultimately results in the destruction of Brønsted acid sites; considered to be crucial for the catalytic conversion of NO_x. In the presence of SO_2 however, enhanced catalytic activity was observed which was suggested to be a result of the formation of additional Brønsted sites (S-OH) via a surface bidentate sulfate intermediate species. The formation of these species was attributed to the interaction of Pb with SO_2 and O_2 on the surface of the catalyst. Density functional theory (DFT) calculations based on a monolayer V model on TiO_2 (0 0 1) showed that SO_2 absorbed selectively onto Pb sites rather than V or Ti oxides. It was subsequently determined that NH_3 absorption proceeds through the formation of Pb-N species with Pb atom and H-O with SO_2. We believe that the present work provides new insights into the design and application of SCR catalysts with specific relevance for application in flue gas streams which contain high quantities of Pb content.

Corresponding authors at: Department of Environmental Science and Engineering, State Key Laboratory of Multiphase Flow in Power Engineering, School of Energy and Power Engineering, Xi'an Jiaotong University, Xi'an 710049, PR China (C. He).

E-mail addresses: chi_he@xjtu.edu.cn (C. He), jschen@iue.ac.cn (J. Chen).

1. Introduction

The selective catalytic reduction of NO_x by NH_3 (NH_3-SCR) is one of the most popular methods for the removal of NO_x from stationary sources. Though V_2O_5-WO_3/TiO_2 displays excellent activity in NH_3-SCR and is the predominantly the main commercial catalyst for this process, many compounds containing alkali/alkali earth metal elements, Pb, Zn, As or Cl are commonly found in flue gas streams, can lead to the de-activation of V_2O_5-WO_3/TiO_2 catalysts [1–4]. In addition to the pre-viously mentioned composite species, SO_2 is also a common component of many industrial flue gas streams where the combustion of sulfur-containing fuels occurs. As such, these species have an important in-fluence on the performance of SCR catalysts [5–8]. Much of the pre-vious research investigating the mechanisms of deactivation of SCR catalysts are conducted in the absence of SO_2, which may limit the understanding of the deactivation pathways of SCR catalysts under real conditions. Recent work conducted by Khodayari and Odenbrand sug-gested that sulfation by SO_2 increased the activity of deactivated SCR catalysts used in bio fuel plants [9,10]. Subsequent work by Yu et al. and Li et al. investigated the deactivation of poisoned catalysts under gas mixtures containing SO_2 and found a number of interesting results [11,12]. Yu et al. proposed that the presence of SO_2 in these streams assisted with the regeneration of acid sites on the catalysts surface, resulting in an increase in the activity of K-poisoned catalysts [11]. Interestingly, Li and co-workers showed that SO_2 lead to more sig-nificant reductions in activity with K-poisoned catalysts due to the formation of $K_2S_2O_7$. It was proposed that this reduction in performance was a result of the $K_2S_2O_7$ species inhibiting the adsorption of NH_3, which was subsequently found to weaken the oxidative ability of cat-alysts [12]. Investigations into the influence of SO_2 on catalysts poi-soned by other elements however, are somewhat limited. This leaves a large portion of the field somewhat untouched, as a significant amount of understanding can still be acquired from assessing how these other additives effect the commercial NH_3-SCR catalyst under real operating conditions. Such knowledge and understanding may provide critical insights for the future design and optimization of this material for NH_3-SCR reaction.

The quantity of waste incineration plants being built has increased significantly in recent years. A significant quantity of these utilize NH_3-SCR technology to abate NO_x. Due to the large quantities of Pb which are typically found in these waste streams, up to 3350 ppm of Pb can build up on the surface of these catalysts after running for only running 1908 h in a waste incinerator [13,14]. Gao et al. recently discovered that Pb atoms cover V active sites and typically caused a decrease in the population of acid sites in SCR catalysts [15]. Additionally, Peng et al. subsequently investigated the Pb deactivation mechanism on CeO_2-WO_3 for NH_3-SCR and found that Pb caused the loss of surface acidity by covering WeO and W]O [14]. Whilst, it was very much agreed that Pb reduced the quantity of acid sites in these catalysts, these experi-ments were all conducted in the absence of SO_2.

Density Functional Theory (DFT) is an efficient method which can be utilized to study the deactivation mechanisms of catalysts [16–18]. As a consequence, DFT and experimental methods were both employed to investigate the influence of SO_2 on Pb-poisoned SCR catalysts in this study. Results revealed that SO_2 reacted with Pb species to form surface bidentate sulfate on poisoned catalysts rather than V or Ti oxides, and the new forming surface sulfate could perform as Brønsted acid sites and increased the activity of poisoned catalyst remarkably.

2. Experimental section

2.1. Catalyst preparation

Commercial V_2O_5-WO_3/TiO_2 (shortened to V-Ti) which is obtained from a coal-fired power plant was used in this investigation. As com-monly used by most researchers, a wet impregnation method was used to prepared the Pb-poisoned sample [14,19]. For this, 0.2 M $Pb(NO_3)_2$ was prepared and V-Ti sample was impregnated by the solution for 2 h. The resulting material was subsequently filtered, washed with deio-nized water and dried at 120 °C for 3 h. The dried sample was subse-quently calcined 500 °C in air for 3 h. The concentrations of Pb and V in the synthesized sample were measured by inductively coupled plasma-optical emission spectrometer (ICP-OES) and the calculated atomic ratio of Pb/V was found to be 0.41 for Pb-V sample.

2.2. NO_x conversion tests

NO_x conversion of the prepared catalysts was tested in a fixed-bed quartz reactor (Φ 8 mm × 400 mm). All samples were ground using a 20–40 mesh and 1.2 mL of each sample was placed in the reactor. For

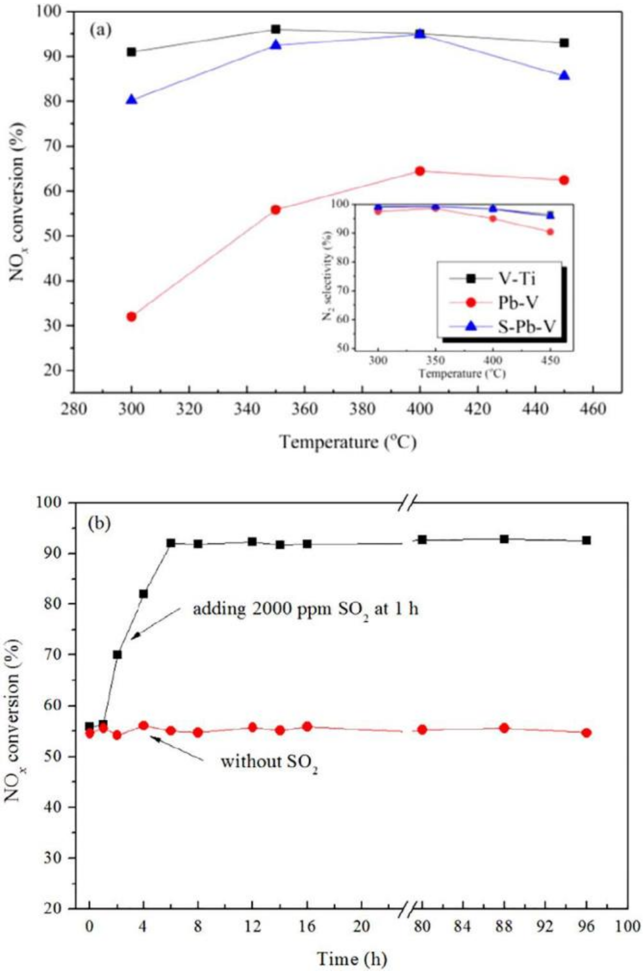

Fig. 1. (a) SCR performance of V-Ti, Pb-V and S-Pb-V sample (Reaction condition:

(b) The influence of SO_2 on activity of Pb-V sample at 350 °C.

Table 1

Specific surface area (S_{BET}), pore volume (V_p), average pore radius (r_p) and total amount of acid sites (T_{acid}) of catalysts.

Sample	S_{BET} (m^2/g)	V_p* (cm^3/g)	r_p (nm)	T_{acid} (mmol/g)
V-Ti	83.7	0.2994	7.2	0.445
Pb-V	80.7	0.2956	7.3	0.073
S-Pb-V	80.3	0.2955	7.4	0.283

* Obtained at P/P_0 = 0.99.

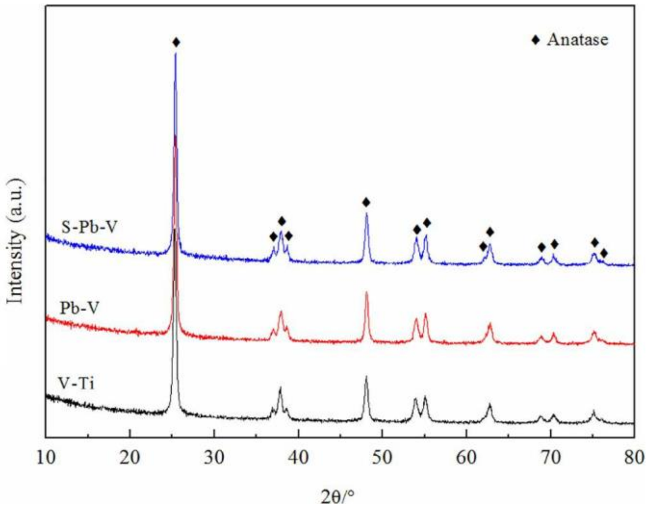

Fig. 2. XRD results of V-Ti, Pb-V and S-Pb-V sample.

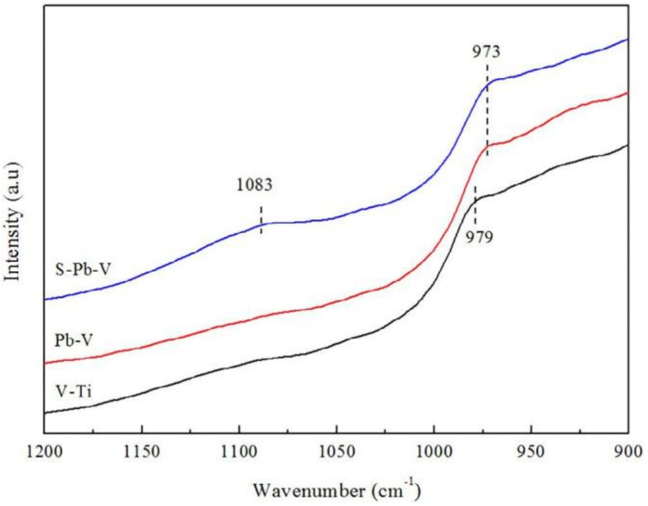

Fig. 3. Raman spectra of V-Ti, Pb-V and S-Pb-V sample.

Table 2

The concentration variations of V, Pb and S elements on Pb-V sample during the process of sulfation (10^{-3} g/g).

Element	0 h	1 h	3 h	8 h	16 h	48 h	96 h
V	8.41	8.49	8.27	8.46	8.51	8.37	8.28
Pb	13.99	13.02	14.71	14.25	13.56	13.41	13.26
S	1.21	2.01	8.78	12.21	12.65	12.89	13.42

these tests, N_2 was used as the inert carrier and the typical feed con-tained NO (500 ppm), NH_3 (500 ppm), SO_2 (2000 ppm when stated), H_2O (5.0 vol%) and O_2 (4.0 vol%). The total gas flow rate used was 1200 mL/min which corresponded to a gas hourly space velocity (GHSV) of 60,000 h^{-1}. Concentrations of O_2, SO_2, NO and NO_2 in ga mixture at the inlet and outlet were analyzed using a T-350 flue gas analyzer (Testo Company, Germany) and concentration of N_2O was analyzed using a SENMA IR Sensor (Madur Company, Austria). For each reaction, the NO_x conversion (x) and N_2 selectivity (S_{N_2}) was calculated by Eqs. (1) and (2), respectively:

$$x = \frac{C_{NO_{x,in}} - C_{NO_{x,out}}}{C_{NO_{x,in}}} \times 100\% \qquad (1)$$

$$S_{N_2} = 1 - \frac{2C_{N_2O}}{C_{NO_{x,in}} - C_{NO_{x,out}}} \times 100\% \qquad (2)$$

where $C_{NO_{x,in}}$ and $C_{NO_{x,out}}$ were the concentrations of NO_x observed (NO + NO_2) in the inlet and outlet of the reactor, respectively. And C_{N_2O} was the concentration of N_2O observed in the outlet of the reactor.

2.3. Catalyst characterizations

N_2 adsorption-desorption isotherms of catalyst samples were col-lected at −196 °C on a NOVA 2000e surface area and pore size analyzer (Quantachrome, USA). Powder X-ray diffraction (XRD) was performed using an X'Pert Pro XRD diffractometer (PANalytical B.V., Holland) with Cu Kα radiation. X-ray photoelectric spectroscopy (XPS) was conducted using an ESCALAB 250 spectrometer (Thermo Fisher Scientific Company, USA) with Al Kα radiation. Raman spectra were collected on a Laser Raman spectrometer (LabRAM Aramis, HORIBA Jobin Yvon, France). Catalyst sample (0.05 g) was dissolved in a mix-ture solution of HNO_3 (5 mL) and HF (0.5 mL), and then the con-centrations of V, Pb and S elements were measured by ICP-OES (Optima 7000DV, PerkinElmer, USA). The temperature programmed reduction in H_2 (H_2-TPR) and temperature-programmed desorption of NH_3 (NH_3-TPD) was conducted using a ChemBET-3000 TPR-TPD chemisorption analyzer (Quantachrome, USA) [20].

In situ diffuse reflectance infrared Fourier transform spectroscopy (In situ DRIFTS) was conducted using a Bruker Vertex 70 (Bruker, Germany) infrared spectrometer. For these experiments, the powdered sample was placed in the reaction cell (Harrick Scientific) and initially treated under N_2 at 400 °C for 1 h to remove any surface impurities. Then the reaction cell was subsequently cooled to 350 °C and a back-ground spectrum was recorded. Once the background spectrum was recorded, the stated gas mixture was introduced into the cell and the resulting spectra were recorded.

2.4. DFT calculation

The first-principle density functional theory calculations (including structural and electronic investigations), were performed based on the Cambridge Sequential Total Energy Package (CASTEP) [21]. The elec-tron-electron interaction was described by the exchange-correlation functional under the generalized gradient approximation (GGA) [22], with norm-conserving pseudopotentials and Perdew-Burke-Ernzerh of functionality [23]. An energy cutoff of 750 eV was used and a k-point sampling set of 5 × 5 × 1 were tested for convergence. A force toler-ance of 0.01 eV $Å^{-1}$, energy tolerance of 5.0×10^{-7} eV per atom and maximum displacement of 5.0×10^{-4} Å were considered. Each atom in the storage models was allowed to relax to the minimum in the en-thalpy without any constraints. The vacuum space along the z direction was set to be 15 Å, which was enough to avoid interaction between the two neighboring images. The adsorption energy of NH_3 (E_{ads}) on the surface of substrates was defined as:

$$E_{ads} = E_{*NH_3} - (E_{*} + E_{NH_3}) \qquad (3)$$

where $*NH_3$ and $*$ denoted the adsorption of NH_3 on substrates and the bare substrates, respectively. E_{NH_3} denoted the energy of NH_3 mole-cular.

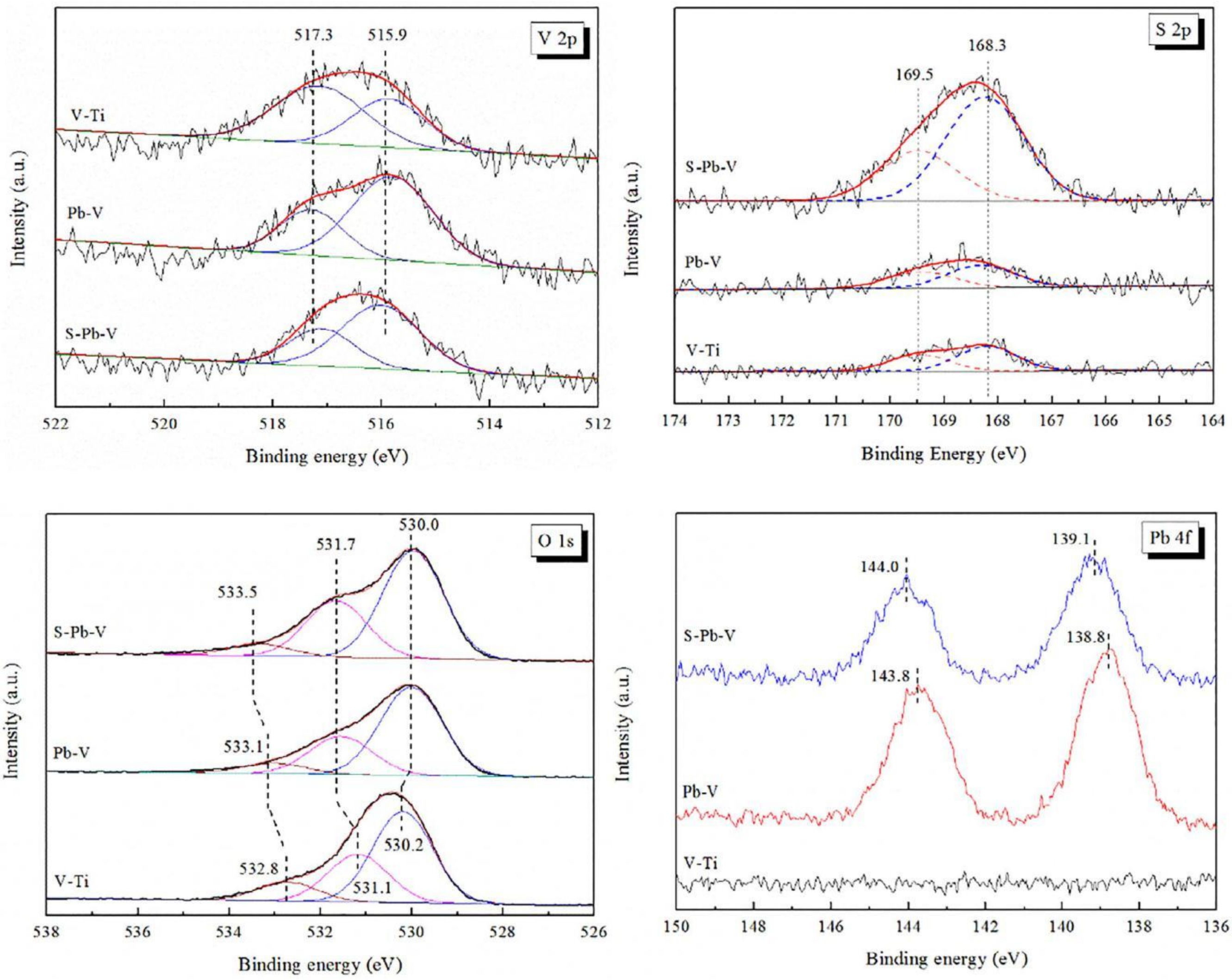

Fig. 4. XPS spectra of V 2p, S 2p, O 1s and Pb 4f for V-Ti, Pb-V and S-Pb-V sample.

Table 3
XPS results of O 1s for each catalyst sample.

Sample	O_α	O_β	O_γ
V-Ti	530.2 (59.7)	531.1 (30.4)	532.8 (9.9)
Pb-V	530.0 (64.5)	531.7 (26.3)	533.1 (9.2)
S-Pb-V	530.0 (54.2)	531.7 (38.8)	533.5 (7.0)

O_α: lattice oxygen, O_β: OH group, O_γ: adsorbed oxygen. Data in parentheses mean ratio of O_α, O_β and O_γ to $O_\alpha + O_\beta + O_\gamma$ (%).

3. Results and discussion

3.1. NO_x conversion over catalysts

The calculated NO_x conversion and N_2 selectivity of all the syn-thesized catalysts can be found in Fig. 1a. It was determined that the commercial V_2O_5-WO_3/TiO_2 displayed high catalytic activity under testing conditions and NO_x conversions in excess of 90% with N_2 se-lectivity in excess of 95% were observed at temperatures ranging from 300 to 450 °C. As anticipated, a significant loss in performance was observed with the Pb-poisoned sample, as the highest NO_x conversion observed for this catalyst was only 64.3% at 400 °C, which was sub-stantially lower than the fresh sample at the same conditions (94%). The N_2 selectivity of Pb-poisoned sample was also decreased. The in-hibiting effect of Pb on the performance of this material as an SCR catalyst aligned well with results reported in previous publications [19,24].

The influence of SO_2 on the activity of Pb-poisoned sample was subsequently assessed and the corresponding results from this in-vestigation are displayed in Fig. 1b. The Pb-poisoned sample main-tained a NO_x conversion of approximately 55% under 350 °C for 96 h. Interestingly, when SO_2 (2000 ppm) was added to the gas feed at 350 °C, the NO_x conversion over the Pb-poisoned sample increased significantly with the time and appeared to be stable at approximately 92% the end of the experiment. The NO_x conversions observed over the Pb-poisoned sample after sulfation by SO_2 (S-Pb-V) was also in-vestigated over 96 h and the corresponding data can be found in Fig. 1a. At most of the temperatures assessed, the NO_x conversion exhibited by the S-Pb-V was found to be higher than the Pb-V material. At 400 °C, NO_x conversion over the S-Pb-V material increased to 94%, which was similar to the performance exhibited by the fresh commercial catalyst. The N_2 selectivity of the S-Pb-V material was also similar to the fresh commercial catalyst at all test temperatures. As such, it can be con-cluded that the presence of SO_2 in the reactions has a profound effect on the catalytic performance and can remarkably increase the activity of SCR catalysts poisoned by Pb.

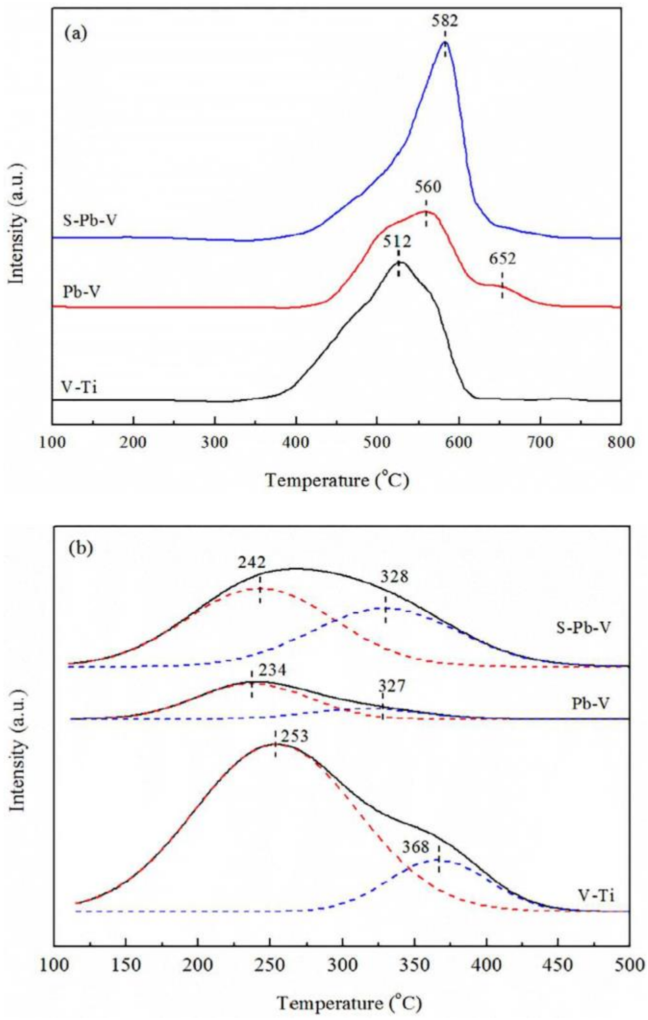

Fig. 5. (a) H_2-TPR and (b) NH_3-TPD profiles of prepared catalysts.

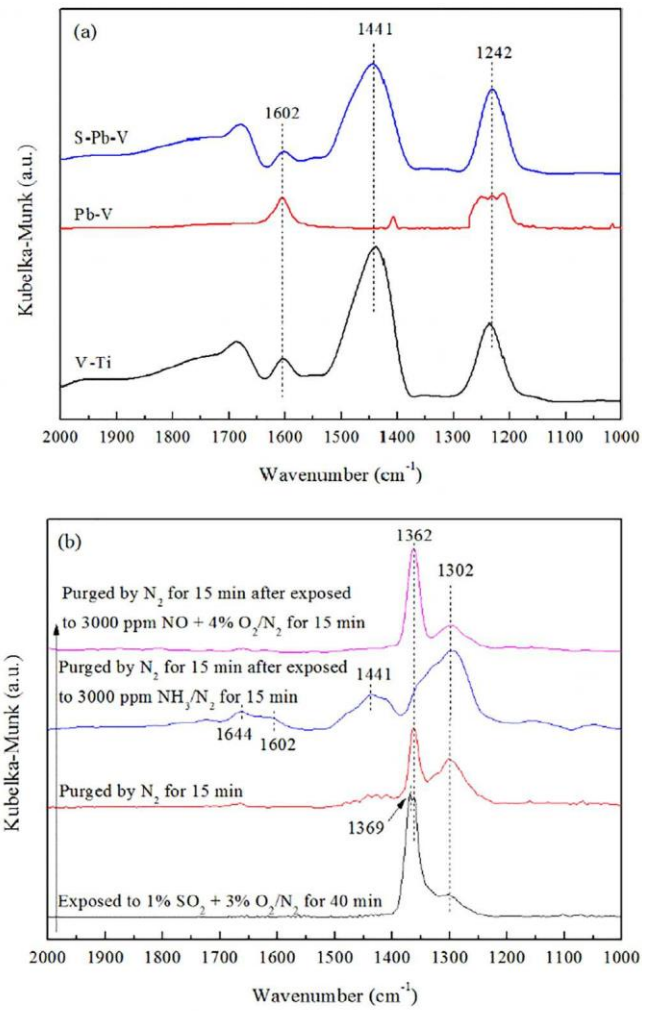

Fig. 6. (a) DRIFTS spectra of samples after adsorbing NH_3 at 350 °C; (b) In situ DRIFTS of Pb-V sample exposed to 1% SO_2 + 3% O_2/N_2, 3000 ppm NH_3/N_2 and 3000 ppm NO + 4% O_2/N_2 in order at 350 °C.

3.2. Characterization of synthesized catalysts

3.2.1. Structural and surface properties

The N_2 adsorption-desorption isotherms and pore size distributions corresponding to V-Ti, Pb-V and S-Pb-V can be found in Fig. S1. In addition, each sample's specific surface area (S_{BET}), total pore volume (V_p) and average pore radius (r_p) can be found in Table 1. It is evident from the characterization of these materials that the deposition of Pb and SO_2 on the surface of the V-Ti material appears to have an insignificant influence on pore structure of the commercial SCR catalyst. The XRD patterns of each of the materials are displayed in Fig. 2. Only diffraction patterns which are typically associated with a TiO_2-anatase phase are observed, which suggests that the deposited Pb is well dispersed in the Pb-V and S-Pb-V materials.

The surface of each material was subsequently probed using Raman spectroscopy, the corresponding spectra of which are displayed in Fig. 3. In the spectra of the V-Ti sample, a small broad peak at 979 cm^{-1} is observed, which is likely to be indicative of a V]O symmetric stretching mode which is commonly observed in polymeric surface vanadia [25,26]. The low intensity observed for this stretching mode is unsurprising, given that the V_2O_5 loadings in such catalysts are typically low (< 1.5 wt%) to reduce the oxidation rate of SO_2 in the system [27]. After doping with Pb (Pb-V material), the corresponding peak undergoes a downward shift to a lower wavenumber (973 cm^{-1}), which has previously been attributed to an interaction between the Pb and V species [28]. With the S-Pb-V sample, a new broad peak at approximately 1083 cm^{-1} appears, which is indicative that surface bound sulfate species are present in this material [20]. The concentration variations of Pb, V, and S elements on Pb-V sample during the process of sulfation were measured by ICP-OES and the results can be found in Table 2. As expected, the concentration of V and Pb elements vary little along with the reaction time, however, the concentration of S increases significantly along with the reaction time, suggesting that sulfate should be formed on the sample.

Fig. 4 shows the XPS spectra of V 2p for the series of materials. It is known that in the commercial catalyst (V-Ti), V is present in two oxidation states; V^{5+} at 517.3 eV and V^{4+} at 515.9 eV [23,29]. The V^{5+}/ V^{4+} ratio of which, is typically about 1.19. Interestingly in the Pb-V material, the proportion of V^{5+} decreases significantly, which leads to a reduced V^{5+}/V^{4+} ratio of approximately 0.48. This suggests that the deposition of Pb to this material significantly reduces the quantity of V^{5+} species in the material [23]. The important relationship between these V^{5+} species and the catalytic performance of these materials in SCR reactions has previously been highlighted. As such, the proportion of V^{5+} species in these materials should be monitored closely when investigating the deactivation of V-based materials for the SCR reaction [30]. Interestingly, with the S-Pb-V material, the ratio of V^{5+}/V^{4+} was calculated to be approximately 0.45 which is comparable with the Pb-V material. This is conclusive evidence suggesting that sulfation of the Pb-V sample does not directly lead to the recovery of V^{5+} species on the materials surface.

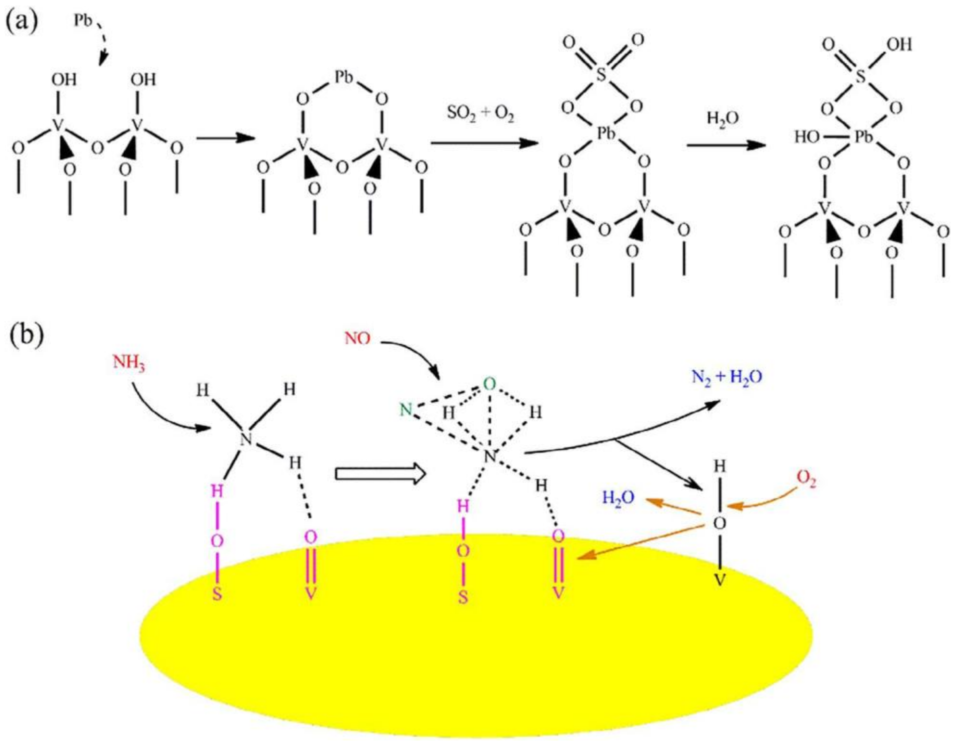

Scheme 1. Formation of Brønsted acid sites (a) and proposed NH_3-SCR reaction route (b) on Pb-poisoned catalyst after sulfation.

It is known that commercial SCR catalysts often contain a small quantity of S [27]. As such, the state of S in the fresh sample was investigated by XPS. Two peaks were observed in the S 2p XPS spectrum of the fresh catalyst (Fig. 4), which centered at 168.3 and 169.4 eV which can be attributed to HSO_4^{1-} and SO_4^{2-} respectively [20,31]. The ratio of HSO_4^{1-}/SO_4^{2-} was subsequently determined to be approximately 1.34 in the fresh catalyst. Similar XPS investigations also carried out with the Pb-V and the S-Pb-V materials. After Pb deposition (Pb-V), the HSO_4^{1-}/SO_4^{2-} ratio was very similar to the fresh sample. However, when this Pb-poisoned sample was subsequently sulfated, the intensity of the S 2p for S-Pb-V sample increased significantly, suggesting that the presence of S containing species on the surface of the materials has increased significantly, which aligns well with the data collected from the Raman spectroscopy and ICP-OES. Furthermore, quantitative analysis of the XPS spectra revealed that the HSO_4^{1-}/ SO_4^{2-} ratio had increased significantly which suggests that S is predominantly present as a HSO_4^{1-} species on the surface of the S-Pb-V material.

Three types of O species were observed in the XPS spectra of the V-Ti sample (Fig. 4). These can be attributed to the lattice oxygen (O_α) of the metal oxides at 530.2 eV, surface OH groups (O_β) at 531.1 eV and weakly adsorbed oxygen (O_γ) at 532.8 eV [32]. It has previously been suggested that due to a strong interaction between Pb and SCR catalysts [23], the peak attributed to O_α shifts to a lower binding energy (530.0 eV) and the location of O_β and O_γ shifts to a higher binding energy (531.7 and 533.1 eV respectively). These characteristic shifts are clearly visible in the XPS spectra of the Pb-V material. Interestingly, after the Pb-poisoned sample was sulfated, the binding energies associated with O_α and O_β did not appear to shift but binding energy associated with the O_γ shifted to 533.5 eV. Concentrations of O_α, O_β and O_γ in all samples are displayed in Table 3. It is clearly evident that the content of O_β in the S-Pb-V sample increases significantly, which may indicate that exposing these materials to SO_2 can increase the population of surface bound OH species.

Fig. 4 shows the Pb 4f spectra of associated with each of the materials. As perhaps one would expect, no significant signal could be assigned to Pb in the fresh sample, suggesting that Pb is only likely to present in exceptionally small quantities in the commercial SCR catalyst. After Pb deposition, two peaks appear at binding energies of 138.8 and 143.8 eV which can be attributed to PbO [23]. In the S-Pb-V material, these peaks were found to shift slightly to higher binding energies (139.1 and 144.0 eV). This shift is indicative of an interaction between Pb and SO_2/O_2 species on the surface of the material [33,34], which consequentially causes the Pb peaks to shift to a higher binding energy.

3.2.2. Reducibility and surface acidity

As mentioned above, the surface reducibility of the V^{5+} species can significantly influence a materials activity in SCR. As such, H_2-TPR was conducted on each of the materials in order to investigate the reducibility of each material. The results of these investigations are displayed in (Fig. 5a). The commercial SCR catalyst (V-Ti) exhibits a broad H_2 consumption peak at a temperature range from 350 to 620 °C, which can be assigned to the reduction of surface V species. Interestingly, when Pb is deposited on the material, this characteristic H_2 consumption appears to take place at a higher temperature and a new shoulder peak centered at about 652 °C appears. Previous work has attributed this to the reduction of an O atom coordinated to Pb [15]. As such, it can be postulated that the doping of Pb decreases surface reducibility which aligns with the results observed in the V 2p spectra of the XPS. The reduction peak observed in the H_2-TPR of the sulfated material (S-Pb-V) is very sharp and is likely a result of the reduction of sulfated surface species.

The adsorption of NH_3 on SCR catalysts is a key step in NH_3-SCR systems. As such, NH_3-TPD was carried out on each of the materials and the corresponding results are displayed in Fig. 5b. The desorption of NH_3 on the commercial SCR catalyst begin at approximately 100 °C and is completely removed from the material at approximately 470 °C. The desorption peaks centered at 253 and 368 °C are associated with medium-strong and strong acid sites respectively. The total amount of acid sites (T_{acid}) on the commercial catalyst was determined to be approximately 0.445 mmol/g (Table 1). By comparison, T_{acid} for the Pb-V and S-Pb-V materials are calculated to be approximately 0.073 and 0.283 mmol/g respectively. As such, it can be concluded that exposing

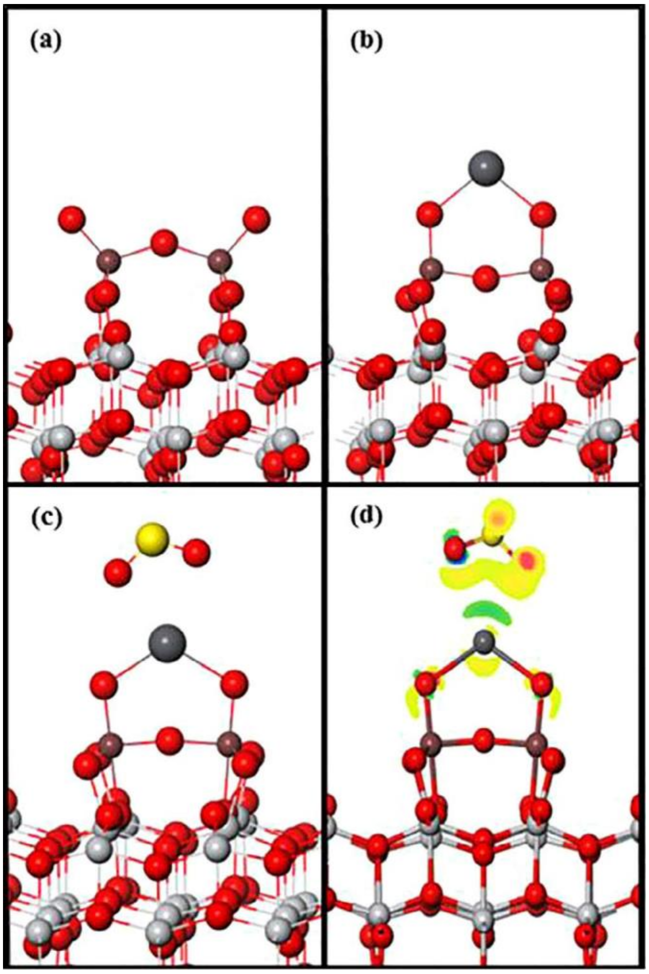

Fig. 7. Optimized structures of (a) V_2O_5/TiO_2, (b) Pb doped on V_2O_5/TiO_2, (c) SO_2 ad-sorbed on Pb-poisoned V_2O_5/TiO_2 and (d) EDD map of SO_2 adsorbed on Pb-poisoned V_2O_5/TiO_2 (Red ball: O atom; Gray ball: Ti atom; Brown ball: V atom; Dark gray ball: Pb atom; Yellow ball: S atom). (For interpretation of the references to colour in this figure legend, the reader is referred to the web version of this article.)

the Pb-V material to SO_2 significantly increases the number of acid sites on the surface of the Pb-V material.

In situ DRIFTS spectra of each material adsorbing NH_3 are shown in Fig. 6a. With the V-Ti material, three bands centered at approximately 1242, 1441, and 1602 cm^{-1} and a broad band from 1650 to 1900 cm^{-1} can be observed. The band at 1441 cm^{-1} and the broad band can be attributed to NH_4^+ on Brønsted acid sites on the surface of the material [35,36]. Additionally, the bands at 1602 and 1238 cm^{-1} could be as-signed to NH_3 on Lewis acid sites and $-NH_2$ wagging species respec-tively [11,20]. With the poisoned sample (Pb-V), a significant reduction was observed for the band at 1441 cm^{-1}, suggesting that the Brønsted acid sites on the surface of the material are poisoned by the Pb, which is likely due to the reaction of V-OH species with the Brønsted acid sites. The intensity of the band at 1602 cm^{-1} however, did not show a sig-nificant change after Pb doping, which implies that Pb does not affect the Lewis acid sites. Given that NH_3 such a significant deactivation is observed in the activity of this material after doping with Pb, it can be postulated that the Brønsted acid sites are crucially important for cat-alytic activity in these systems, which is in correlates with previous investigations [23]. Interestingly, for the S-Pb-V material, the band at 1441 cm^{-1} appeared to increase once again (albeit slightly lower than that observed with the V-Ti material). Nevertheless, this suggests that sulfation of the Pb-V material leads to the formation of new Brønsted acid sites on the Pb-poisoned sample. As discussed previously, the XPS data suggested that sulfation leads to the formation of a large quantity of surface-bound OH species. Given, that the sulfonated material ex-hibits such an increased in Brønsted acidity, it can be postulated that this increased in Brønsted acidity is a result an increased population of S-OH species on the materials surface, which corresponds with previous work in this area [20,37]. As such, it can be concluded that this increase in the number of Brønsted acid sites is responsible for the enhanced performance observed with the sulfonated Pb-poisoned catalyst.

3.2.3. In situ DRIFTS of Pb-V sample under $SO_2 + O_2$

Fig. 6b shows the results obtained from an in situ DRIFTS in-vestigation of the Pb-V sample after exposure to $SO_2 + O_2$, NH_3 and $NO + O_2$ respectively. When the sample was exposed to the 1% SO_2 + 3% O_2/N_2 blend for 40 min, bands at 1369, 1362 and 1302 cm^{-1} were observed, which are characteristic bands associated with the asymmetric stretching frequencies of O]S]O in surface bidentate sulfate species [5,38,39]. After purging the cell with N_2 for an addi-tional 15 min, the bands at 1362 and 1302 cm^{-1} were still visible, suggesting that the newly formed surface bidentate sulfate species is stable. The sample was subsequently exposed to NH_3 (3000 ppm) for 15 min and purged by N_2 for an additional 15 min. Interestingly, bands at 1644 and 1441 cm^{-1} (which can be typically assigned to NH_4^+ species chemisorbed on Brønsted acid sites) appeared. This suggests that the formation of the surface bidentate sulfate species act as an intermediate species in the formation of the new Brønsted acid sites. Finally, the sample was exposed to a blend of NO + O_2 for 15 min and once again purged by N_2 for 15 min. All the bands which had previously been attributed to the adsorption of NH_3 had disappeared but the bands assigned to the surface bidentate sulfate species were still observable. This implies that the NH_4^+ species absorbed on the Brønsted acid sites take part in SCR reaction and that the surface bidentate sulfate species is not consumed in the reaction. As such, it can be proposed that the NH_3-SCR reaction on Pb-poisoned catalysts follow the Eley-Rideal me-chanism after exposure to SO_2. Brønsted acid sites forming on the Pb-poisoned catalyst after sulfation are likely formed via the pathway proposed in Scheme 1a. Additionally, the NH_3-SCR reaction on a sul-fated Pb-poisoned catalyst may proceed via the pathway displayed in Scheme 1b.

3.3. DFT calculations

Optimized structures of the V-Ti, Pb-V and S-Pb-V materials are shown in Fig. 7. For V_2O_5-WO_3/TiO_2 SCR catalysts, it is widely ac-knowledged that WO_3 acts as a promoter and V models or V models on TiO_2 are predominantly used in theoretical calculations [15,35]. For the reasons discussed previously, V loadings in SCR catalysts are typically low and thus, V species should exit on catalysts as monolayer. A similar approach to other previous studies was utilized here [40], where the monolayer V model on TiO_2 (0 0 1) was calculated (As depicted in Fig. 7a). Using this methodology, the V]O and VeOeV bond lengths were calculated to be approximately 1.810 Å and, 1.889 to 1.903 Å respectively. After Pb doping on the surface is achieved, it was observed that Pb atoms can coordinate to V species (Fig. 7b), as shown in a previous study [15]. The calculation result for the SO_2 adsorbed on Pb-poisoned material is shown in Fig. 7c and the electron density differ-ence (EDD) mapping is shown in Fig. 7d. In the EDD maps, the red and yellow regions correspond to electron accumulation and blue and green regions correspond to regional electrons loss. Free electrons in the Pb atom are transferred to the O atom of SO_2. As such, it can be concluded that it's likely that SO_2 predominantly adsorbs on Pb atom rather than V or Ti atoms, which is in agreement with the result of XPS discussed previously.

The adsorption of NH_3 on each optimized structure was subse-quently calculated, the results of which can be found in Fig. 8a–c. The corresponding EDD maps of all three materials are displayed in Fig. 8d–f. From these calculations, it appears that the NH_3 preferentially adsorbs on the top of a V_2O_5 species via a HeO bond in the commercial

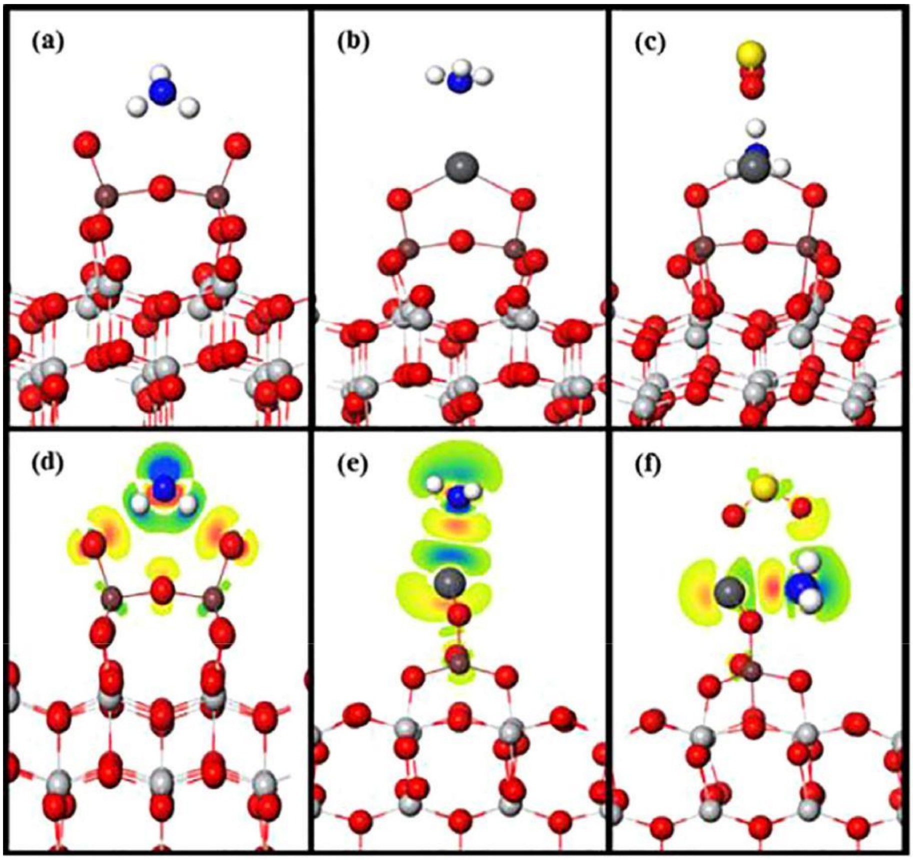

Fig. 8. Optimized configurations of NH_3 adsorption on (a) V_2O_5/TiO_2, (b) Pb doped V_2O_5/TiO_2, (c) Sulfated Pb-poi-soned V_2O_5/TiO_2 and corresponding EDD maps (d and e) (Red ball: O atom; Gray ball: Ti atom; Brown ball: V atom; Dark gray ball: Pb atom; Yellow ball: S atom; Blue ball: N atom; White ball: H atom). (For interpretation of the refer-ences to colour in this figure legend, the reader is referred to the web version of this article.)

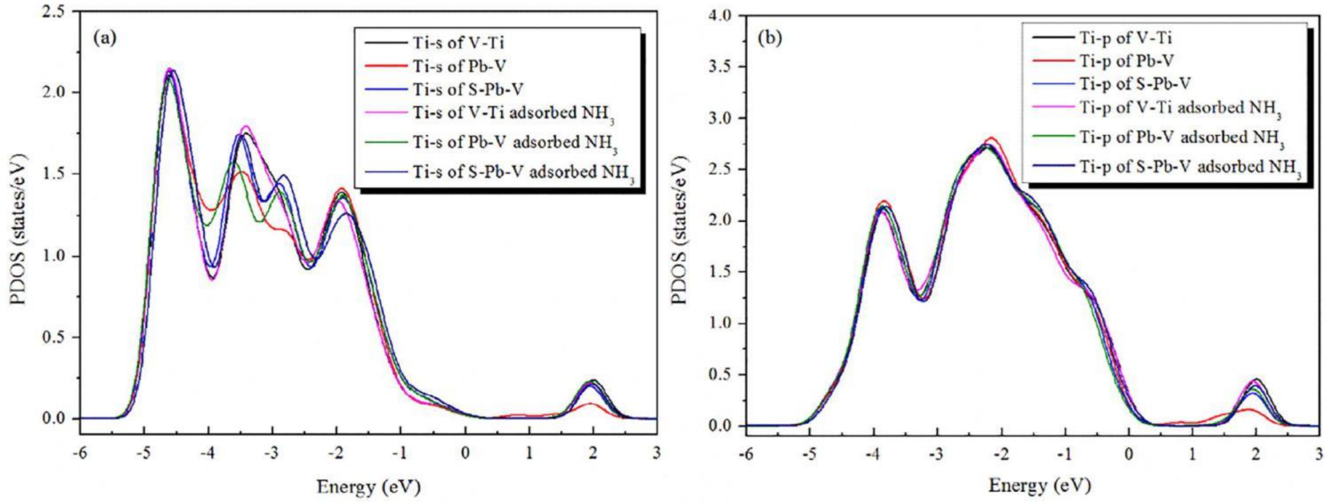

Fig. 9. PDOS analysis of Ti orbitals in all models: (a) s-orbital; (b) p-orbital for Ti.

catalytic material. The free electrons from the blue and green regions of the H atoms are transferred to the red and yellow regions of O atoms (Fig. 8d). Adsorption energy (E_{ads}) of NH_3 on the surface of V_2O_5/TiO_2 was also calculated and E_{ads} was determined to be approximately −0.11 eV. With the Pb-poisoned model, it was determined that NH_3 preferentially adsorbs on the top of both the V_2O_5 and Pb atom via an NePb bond in a bridging like manner. In this case, the free electrons from the blue and green regions of N and Pb atoms transferred to the red and yellow regions of the middle of NePb bond (Fig. 8e). The E_{ads} of NH_3 on the Pb-poisoned sample was subsequently calculated to be approximately −0.90 eV, which suggests that adsorption of NH_3 onto the Pb-poisoned sample is more stable. Peng et al. studied the adsorption of NH_3 on an As-poisoned SCR catalyst and also found that As can strengthen adsorption energy of NH_3 on surface [35]. For the sulfated Pb-poisoned model, NH_3 was found to preferentially adsorb on the side of V_2O_5 + Pb group via a covalent NePb bond due to the presence of surface bound SO_2 species. In this case, the free electrons from the blue and green regions of the N and Pb atoms are transferred to the red and yellow regions in the middle of NePb bond. Free elec-trons from the blue and green regions of H atoms in NH_3 are also transferred to the red and yellow regions of O atoms in SO_2 (Fig. 8f). Once again, the E_{ads} of NH_3 in the sulfated Pb-poisoned sample was calculated and found to be approximately −0.70 eV, indicating that the adsorption of NH_3 in this system was not as stable as in the Pb-poisoned

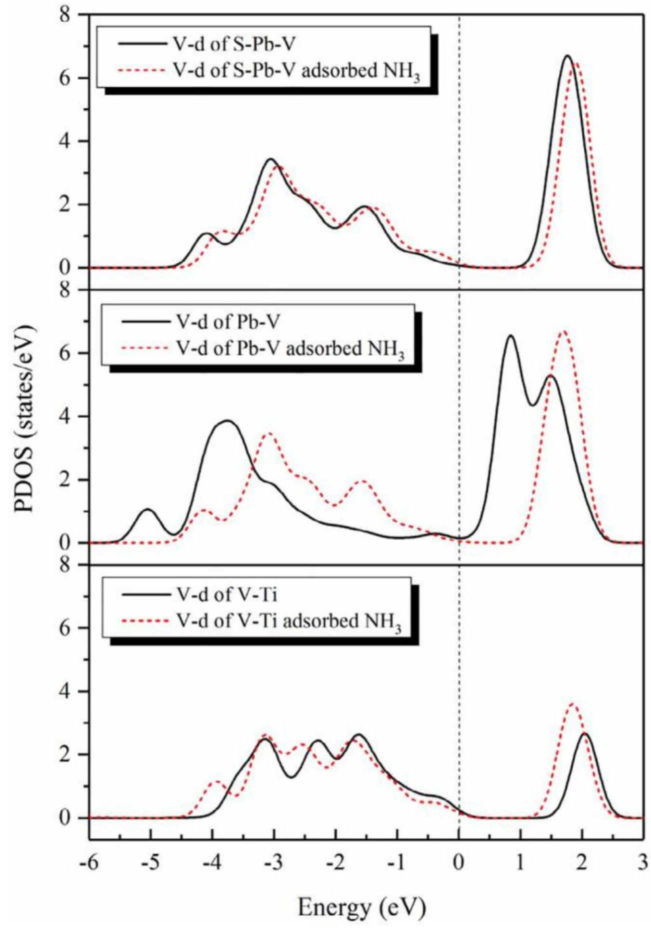

Fig. 10. PDOS of V d-orbital before and after adsorbed NH$_3$.

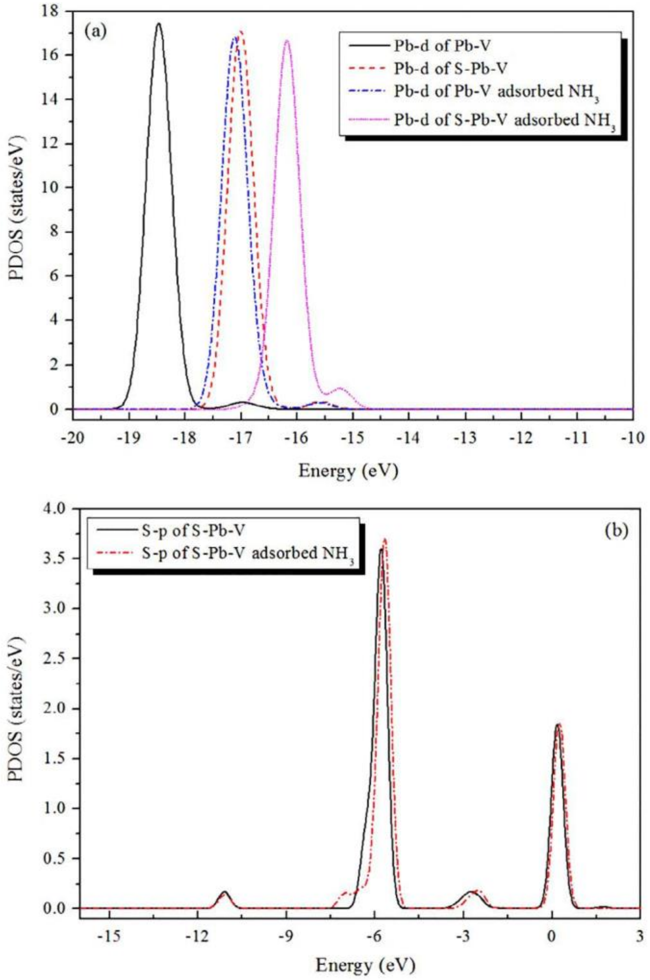

Fig. 11. PDOS of (a) Pb d-orbital and (b) S p-orbital before and after adsorbed NH$_3$.

model system. As such, it can be concluded that the adsorption of SO$_2$ on the surface of Pb-poisoned material has a large influence on ad-sorption mode of NH$_3$ on catalysts surface, which aligns with the earlier discussions regarding the NH$_3$-TPD and in situ DRIFTS data.

Projected density of states (PDOS) analysis was subsequently adopted to verify the interaction between corresponding atoms in the system. The PDOS results which correspond to the s-orbital of Ti in the system are displayed in Fig. 9a. It is evident that a small shoulder peak appears at approximately −2.9 eV in the PDOS of the s-orbital after Pb is deposited onto the surface of the V$_2$O$_5$/TiO$_2$ model system. However, there was no notable difference between the p- and d-orbitals of Ti (Figs. 9b and S2) after the Pb deposition suggesting that the interaction between Pb and Ti atoms was relatively weak. In the S-Pb-V model system, the shoulder peak in PDOS Ti s-orbital became more defined, whilst again no significant change was observed in the PDOS p- and d-orbitals (Figs. 9b and S2). As such, it can be concluded that the SO$_2$ on the surface of the Ti presents very little change to the electronic structure of the Ti and so, it's unlikely that SO$_2$ has a strong interaction with Ti atoms in the system. The influence of NH$_3$ on the Ti atom was also investigated. The NH$_3$ was found to have very little influence on the nature of the s, p and d orbitals in all of the model systems, sug-gesting that NH$_3$ does not interact with Ti directly in the system.

The PDOS results for the d-orbital of V are displayed in Fig. 10. In the valence band region, three peaks at −1.6, −2.3 and −3.1 eV are observed in addition to a shouldered peak observed at −0.3 eV with the V-Ti model system. In the conduction band region, a peak at 2.1 eV appeared. As expected, the PDOS results for the V d-orbital changed drastically after the introduction of Pb to the system. The peak observed in conduction band region split into two defined peaks and both peaks shifted to a lower energy. In the valence region, the peak observed at −1.7 eV almost disappeared completely and the other two peaks also shift to a lower energy (−3.8 and −5.0 eV). It is evident from these results that the doping of Pb has a strong influence on electrons of the V in the model system. Interestingly, after the SO$_2$ was incorporated into the model, only one peak at 1.8 eV is observed in the conduction band region. In valence band region however, three peaks at −1.5, −3.0 and −4.2 eV are observed. This suggests that the adsorption of SO$_2$ on Pb atom may weaken the interaction between the Pb and V.

The influence of NH$_3$ on V d-orbital in each model system was subsequently investigated. With the V-Ti model system, the peaks ob-served at 2.1, −1.7 and −2.3 eV appeared to shift to 1.9, −1.8 and −2.5 eV and a new peak at −3.9 eV appeared, suggesting that NH$_3$ has a strong interaction with V. Interestingly, when the adsorption of NH$_3$ was investigated on the Pb-V model, all the PDOS were found to shift to a higher energy, suggesting that the adsorption of NH$_3$ weakens the interaction between the Pb and V in the system. The results in the sulfated model system were very similar to these, implying that in both cases, the adsorption of NH$_3$ in the system weakens the interaction between the Pb and V. Similar observations were made with the s- and p-orbitals of V for these systems (Fig. S3), which further supports the conclusions made.

The PDOS results corresponding to the d-orbital for Pb in the Pb-V and S-Pb-V systems are displayed in Fig. 11a. A large peak is observed at −18.5 eV and a smaller peak at −16.9 eV for the Pb-V model system. After the incorporation of SO$_2$ to the Pb-V system, the main peak and the smaller peak appeared to shift to a higher energy (−17.0 eV and −15.6 eV respectively). This suggests that there is a strong interaction between the SO$_2$ surface species and the Pb atom. When NH$_3$ was absorbed onto the Pb-V sample, the large peak shifted to −17.2 eV and the smaller peak to −15.6 eV, implying that the interaction between NH_3 and Pb is strong. After NH_3 was absorbed on S-Pb-V model, the large peak shifted to −16.2 eV and the smaller peak to −15.2 eV. As such, it can be suggested that the adsorption of NH_3 likely enhances the influence of SO_2 on Pb, implying that NH_3 was absorbed with SO_2 and Pb. PDOS results of s- and p-orbital for Pb in Pb-V and S-Pb-V model systems also provided further evidence for this conclusion (Fig. S4).

Fig. 11b reveals the influence of NH_3 on PDOS results of p-orbital for S in S-Pb-V model. A large peak is observed −5.8 eV with two smaller peaks observed at −2.9 and −10.8 eV. As NH_3 was absorbed onto the S-Pb-V model, the large peak at −5.8 eV clearly split into two separate defined peaks; one main peak at −5.6 eV and a shoulder peak at −6.9 eV, implying that the interaction of NH_3 and S atoms was strong. PDOS results for the s-orbital for S also suggested the same conclusion (Fig. S5). To conclude, the PDOS analysis of the Ti, V, Pb and S atoms in the model systems suggest that NH_3 likely adsorbs onto the surface sulfate species in the S-Pb-V model.

4. Conclusions

The present study focused on mechanism of SO_2 on activity of Pb-poisoned SCR catalysts with experimental and theoretical method. Pb could react with surface V-OH of commercial SCR catalysts, caused the disappearance of Brønsted acid sites, which should be the main reason for the deactivation of SCR catalysts. SO_2 had a remarkable promotional effect on activity of Pb-poisoned SCR catalysts and NO_x conversion recovered significantly in the presence of SO_2. The results of char-acterization indicated that SO_2 reacted with Pb atoms and formed sulfate on surface of catalysts. The surface sulfate could form new Brønsted acid sites, thus recovered the activity of Pb-poisoned catalysts. From the result of theoretical calculation, it could be easily found that sulfate was formed between SO_2 and Pb, and then NH_3 absorbed on the sulfate through the formation of Pb-N species with Pb atom and HeO with SO_2, in good agreement with experimental results.

Acknowledgements

Financial support from the National Natural Science Foundation of China (21477095, 21677114), National Key Research and Development Program (2016YFC0204201), Natural Science Foundation of Fujian Province, China (2016J05048), General Financial Grant from the China Postdoctoral Science Foundation (2016M602831), Leading Key Research Project for Industry of Fujian Province, China (2015H0043), and Fundamental Research Funds for the Central Universities (xjj2017113).

References

[1] J.H. Li, Y. Peng, H.Z. Change, X. Li, J.C. Rittenden, J.M. Hao, Chemical poison and regeneration of SCR catalysts for NO_x removal from stationary sources, Front. Environ. Sci. Eng. 10 (2016) 413–427.

[2] Y. Liu, Z. Liu, B. Mnichowicz, A.V. Harinath, H.L. Li, B. Bahrami, Chemical deac-tivation of commercial vanadium SCR catalysts in diesel emission control applica-tion, Chem. Eng. J. 287 (2016) 680–690.

[3] H.Z. Chang, J.H. Li, W.K. Su, Y.K. Shao, J.M. Hao, A novel mechanism for poisoning of metal oxide SCR catalysts: base-acid explanation correlated with redox proper-ties, Chem. Commun. 50 (2014) 10031–10034.

[4] W.S. Hu, X. Gao, Y.W. Deng, R.Y. Qu, C.H. Zheng, X.B. Zhu, K.F. Cen, Deactivation mechanism of arsenic and resistance effect of SO_4^{2-} on commercial catalysts for selective catalytic reduction of NO_x with NH_3, Chem. Eng. J. 293 (2016) 118–128.

[5] W.Q. Xu, H. He, Y.B. Yu, Deactivation of a Ce/TiO_2 catalyst by SO_2 in the selective catalytic reduction of NO by NH_3, J. Phys. Chem. C 113 (2009) 4426–4432.

[6] S.J. Yang, Y.F. Guo, H.Z. Chang, L. Ma, Y. Peng, Z. Qu, N.Q. Yan, C.Z. Wang, J.H. Li, Novel effect of SO_2 on the SCR reaction over CeO_2: mechanism and significance, Appl. Catal., B 136–137 (2013) 19–28.

[7] L. Zhang, W.X. Zou, K.L. Ma, Y. Cao, Y. Xiong, S.G. Wu, C.J. Tang, F. Gao, L. Dong, Sulfated temperature effects on the catalytic activity of CeO_2 in NH_3-selective catalytic reduction conditions, J. Phys. Chem. C 119 (2015) 1155–1163.

[8] X.M. Zhou, X.Y. Huang, A.J. Xie, S.P. Luo, C. Yao, X.Z. Li, S.X. Zuo, V_2O_5-decorated Mn-Fe/attapulgite catalyst with high SO_2 tolerance for SCR of NO_x with NH_3 at low temperature, Chem. Eng. J. 326 (2017) 1074–1085.

[9] R. Khodayari, C.U.I. Odenbrand, Regeneration of commercial TiO_2-V_2O_5-WO_3 SCR catalysts used in bio fuel plants, Appl. Catal., B 30 (2001) 87–99.

[10] R. Khodayari, C.U.I. Odenbrand, Regeneration of commercial SCR catalysts by washing and sulphation: effect of sulphate groups on the activity, Appl. Catal., B 33 (2001) 277–291.

[11] Y.K. Yu, J.X. Wang, J.S. Chen, X.R. Meng, Y.T. Chen, H. Chi, Promotive effect of SO_2 on the activity of a deactivated commercial selective catalytic reduction catalyst: an in situ DRIFT Study, Ind. Eng. Chem. Res. 53 (2014) 16229–16234.

[12] Q.C. Li, S.F. Chen, Z.Y. Liu, Q.Y. Liu, Combined effect of KCl and SO_2 on the selective catalytic reduction of NO by NH_3 over V_2O_5/TiO_2 catalyst, Appl. Catal., B 164 (2015) 475–482.

[13] M. Tokarz, S. Järårs, B. Persson, Poisoning of De-NO_x SCR catalyst by flue gases from a waste incineration plant, Stud. Surf. Sci. Catal. 68 (1991) 523–530.

[14] Y. Peng, W.Z. Si, X. Li, J.J. Chen, J.H. Li, J. Crittenden, J.M. Hao, Investigation of the poisoning mechanism of lead on the CeO_2-WO_3 catalyst for the NH_3-SCR re-action via in situ IR and Raman spectroscopy measurement, Environ. Sci. Technol. 50 (2016) 9576–9582.

[15] X. Gao, X.S. Du, Y.C. Fu, J.H. Mao, Z.Y. Luo, M.J. Ni, K.F. Cen, Theoretical and experimental study on the deactivation of V_2O_5 based catalyst by lead for selective catalytic reduction of nitric oxides, Catal. Today 175 (2011) 625–630.

[16] M. Calatayud, C. Minot, Effect of alkali doping on a V_2O_5/TiO_2 catalyst from per-iodic DFT calculations, J. Phys. Chem. C 111 (2007) 6411–6417.

[17] Y. Peng, J.H. Li, W.Z. Si, X. Li, W.B. Shi, J.M. Luo, J. Fu, J. Crittenden, J.M. Hao, Ceria promotion on the potassium resistance of MnO_x/TiO_2 SCR catalysts: an ex-perimental and DFT study, Chem. Eng. J. 269 (2015) 44–50.

[18] Y. Peng, J.H. Li, L. Chen, J.J. Chen, J. Han, H. Zhang, W. Han, Alkali metal poi-soning of a CeO_2-WO_3 catalyst used in the selective catalytic reduction of NO_x with NH_3: an experimental and theoretical study, Environ. Sci. Technol. 46 (2012) 2864–2869.

[19] R. Khodayari, C.U.I. Odenbrand, Deactivating effects of lead on the selective cata-lytic reduction of nitric oxide with ammonia over a V_2O_5/WO_3/TiO_2 catalyst for waste incineration applications, Ind. Eng. Chem. Res. 37 (1998) 1196–1202.

[20] Y.K. Yu, J.F. Miao, J.X. Wang, C. He, J.S. Chen, Facile synthesis of $CuSO_4$/TiO_2 catalysts with superior activity and SO_2 tolerance for NH_3-SCR: physicochemical property and reaction mechanism, Catal. Sci. Technol. 7 (2017) 1590–1601.

[21] M.D. Segall, P.J.D. Lindan, M.J. Probert, C.J. Pickard, P.J. Hasnip, S.J. Clark, M.C. Payne, First-principles simulation: ideas, illustrations and the CASTEP code, J. Phys. Condense. Matter 14 (2002) 2717–2744.

[22] J.P. Perdew, K. Burke, M. Ernzerhof, Generalized gradient approximation made simple, Phys. Rev. Lett. 77 (1996) 3865–3868.

[23] D.R. Hamann, M. Schlüter, C. Chiang, Norm-conserving pseudopotentials, Phys. Rev. Lett. 43 (1979) 1494–1497.

[24] J. Ye, X. Gao, Y.X. Zhang, W.H. Wu, H. Song, Z.Y. Luo, K.F. Cen, Effects of $PbCl_2$ on selective catalytic reduction of NO with NH_3 over vanadia-based catalysts, J. Hazard. Mater. 274 (2014) 270–278.

[25] M. Kobayashi, M. Hagi, V_2O_5-WO_3/TiO_2-SiO_2-SO_4^{2-} catalysts: influence of active components and supports on activities in the selective catalytic reduction of NO by NH_3 and in the oxidation of SO_2, Appl. Catal., B 63 (2006) 104–113.

[26] S.T. Choo, Y.G. Lee, I.S. Nam, S.W. Ham, J.B. Lee, Characteristics of V_2O_5 supported on sulfated TiO_2 for selective catalytic reduction of NO by NH_3, Appl. Catal., A 200 (2000) 177–188.

[27] I. Nova, L.D. Acqua, L. Lietti, E. Giamello, P. Forzatti, Study of thermal deactivation of a de-NO_x commercial catalyst, Appl. Catal., B 35 (2001) 31–42.

[28] H. Kamata, K. Takahashi, C.U.I. Odenbrand, The role of K_2O in the selective re-duction of NO with NH_3 over a V_2O_5(WO_3)/TiO_2 commercial selective catalytic reduction catalyst, J. Mol. Catal. A 139 (1999) 189–198.

[29] Y.K. Yu, C. He, J.S. Chen, L.Q. Yin, T.X. Qiu, X.R. Meng, Regeneration of deacti-vated commercial SCR catalyst by alkali washing, Catal. Commun. 39 (2013) 78–81.

[30] F. Castellino, S.B. Rasmussen, A.D. Jensen, J.E. Johnsson, R. Fehrmann, Deactivation of vanadia-based commercial SCR catalysts by polyphosphoric acids, Appl. Catal., B 83 (2008) 110–122.

[31] H.L. Huang, Y. Lan, W.P. Shan, F.H. Qi, S.C. Xiong, Y. Liao, Y.W. Fu, S.J. Yang, Effect of sulfation on the selective catalytic reduction of NO with NH_3 over γ-Fe_2O_3, Catal. Lett. 144 (2014) 578–584.

[32] C. Guimon, A. Gervasini, A. Auroux, XPS study of the adsorption of SO_2 and NH_3 over supported tin dioxide catalysts used in de-NO_x catalytic reaction, J. Phys. Chem. B 105 (2001) 10316–10325.

[33] E. Godočíková, Z. Bastl, I. Spirovová, P. Baláž, A study of mechanochemical re-duction of lead sulphide by elemental iron on the surface by X-ray photoelectron spectroscopy, J. Mater. Sci. 39 (2004) 3025–3029.

[34] Y. Wang, J. Hu, Q.F. Zhuang, Y.N. Ni, Label-free fluorescence sensing of lead(II) ions and sulfide ions based on luminescent molybdenum disulfide nanosheets, ACS Sustainable Chem. Eng. 4 (2016) 2535–2541.

[35] Y. Peng, J.H. Li, W.Z. Si, J.M. Luo, Q.Z. Dai, X.B. Luo, X. Liu, J.M. Hao, Insight into deactivation of commercial SCR catalyst by arsenic: an experiment and DFT study, Environ. Sci. Technol. 48 (2014) 13895–13900.

[36] F.S. Tang, B.L. Xu, H.H. Shi, J.H. Qiu, Y.N. Fan, The poisoning effect of Na^+ and

Ca^{2+} ions doped on the V_2O_5/TiO_2 catalysts for selective catalytic reduction of NO by NH_3, Appl. Catal., B 94 (2010) 71–76.

[37] Y. Shu, T. Aikebaier, Q. Xie, S. Chen, H.T. Yu, Selective catalytic reaction of NO_x with NH_3 over Ce-Fe/TiO_2-loaded wire-mesh honeycomb: resistance to SO_2 poi-soning, Appl. Catal., B 150–151 (2014) 630–635.

[38] L. Zhang, L.L. Li, Y. Cao, X.J. Yao, C.Y. Ge, F. Gao, Y. Deng, C.J. Tang, L. Dong, Getting insight into the influence of SO_2 on TiO_2/CeO_2 for the selective catalytic reduction of NO by NH_3, Appl. Catal., B 165 (2015) 589–598.

[39] M.H.L. John, Z. Tom, D.C. Peter, SO_2 adsorption and transformations on γ-Al_2O_3 surfaces: a density functional theory study, J. Phys. Chem. C 114 (2010) 10444–10454.

[40] Y. Peng, J.H. Li, W.B. Shi, J.Y. Xu, J.M. Hao, Design strategies for development of SCR catalyst: improvement of alkali poisoning resistance and novel regeneration method, Environ. Sci. Technol. 46 (2012) 12623–12629.